

Electronic Supplementary Information

Theoretical investigation of the adsorption, IR, and electron injection of hydroxamate anchor at the TiO₂ anatase (1 0 1) surface

Wei Li,[†] Luis G. C. Rego,[‡] Fu-Quan Bai,[†] Chui-Peng Kong,[†] and Hong-Xing Zhang^{*,†}

[†] State Key Laboratory of Theoretical and Computational Chemistry, Institute of Theoretical Chemistry, Jilin University, Changchun 130023, People's Republic of China.

[‡] Department of Physics, Universidade Federal de Santa Catarina, Florianópolis, SC 88040-900, Brazil

*E-mail: baifq@jlu.edu.cn; (Fu-Quan Bai) and zhanghx@mail.jlu.edu.cn; (Hong-Xing Zhang)

Figure S1 The anchoring model (a) and TiO₂ anatase (101) surface (b)

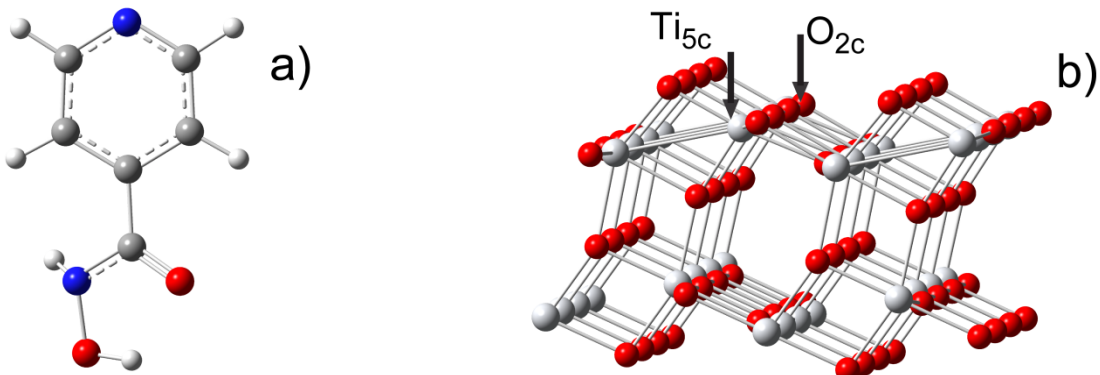
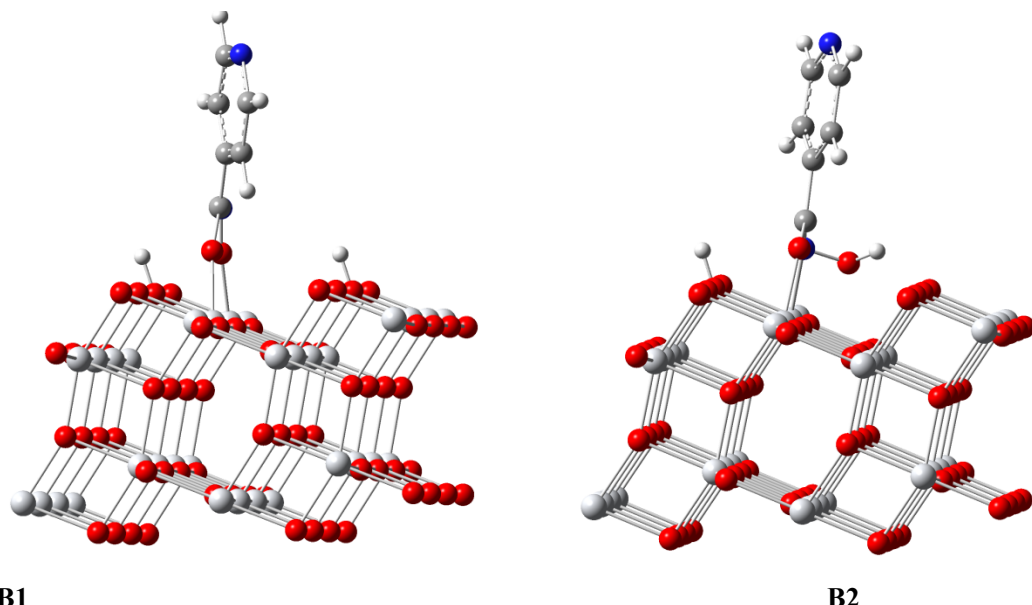
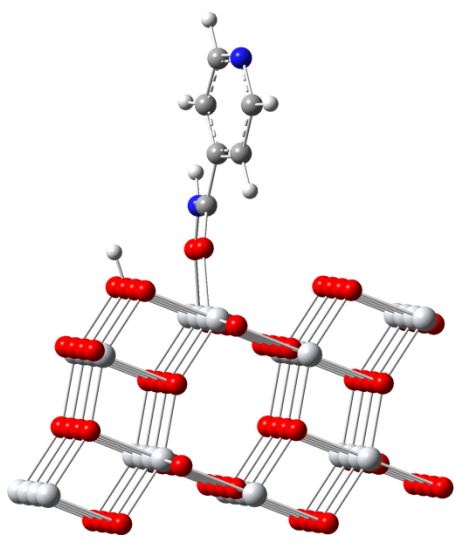
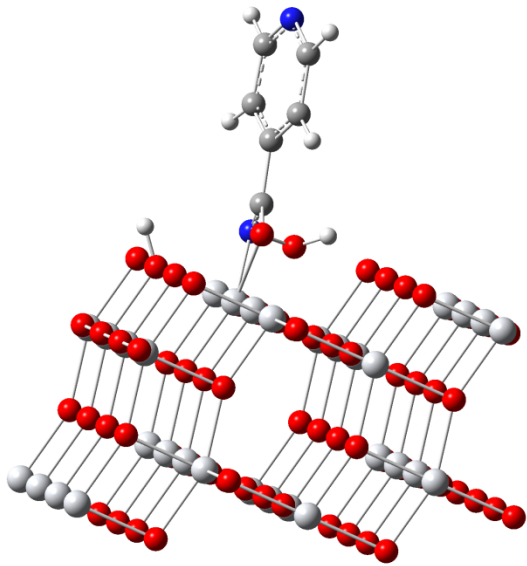


Figure S2 All of the guessed initial structures. The chemically active sites on the surface of anatase (101) are the unsaturated and pairwise arranged acidic cation (Ti_{5c} atoms) and basic anion sites (O_{2c} atoms). There are two possibilities to classify hydroxamate anchor adsorbed on the TiO₂ surface. The first one counts the number of covalent bonds between the adsorbate and the metal atoms of the surface. This can be either monodentate (**M**) or bidentate (**B**) modes. The second one describes the chemistry property of the adsorbate in the adsorption process. This can be either molecular (non-dissociative) or dissociative. In the molecular adsorption process, the hydroxamate anchor is adsorbed on the surface without dissociating. In the dissociative adsorption, the hydroxamate anchor dissociates into the hydroxamate anion and one or two surface bound protons, since both the protons of N-H and O-H in the hydroxamate anchor can be dissociated. It **is worth of noticing that** the dissociated proton can occupy four different bridging oxygen sites. However, as suggested by Nilsing et al.,¹⁻² the choice of where to place the proton did not affect the stability very much, although the geometry is slightly changed during relaxation, and the proton prefers to bind to an under-coordinated surface O_{2c} atom. Configuration **B4** is converted to **M3** during the optimization process.

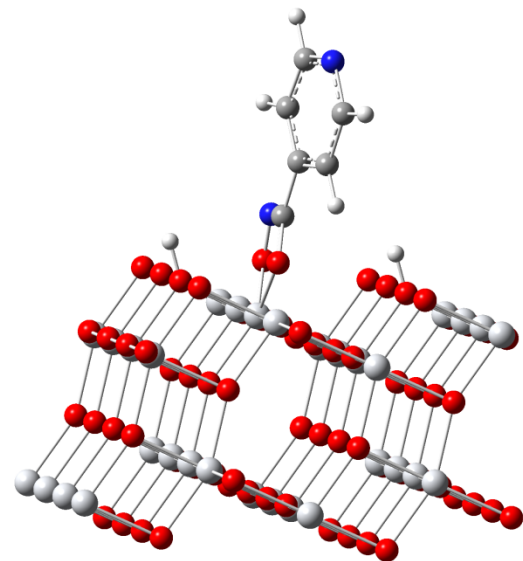




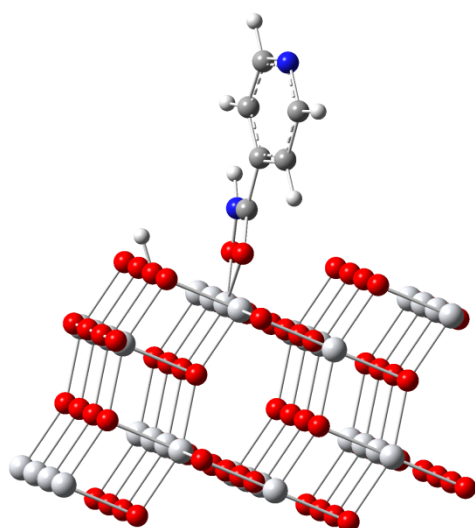
B3



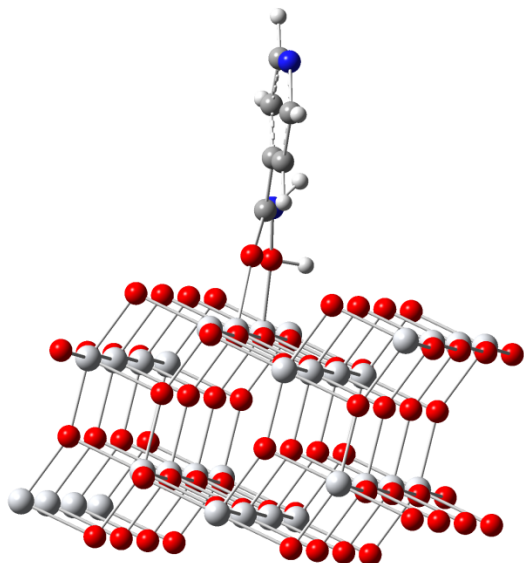
B4



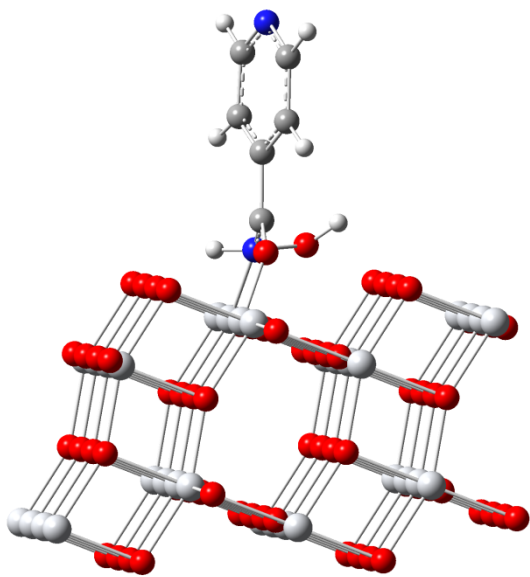
B5



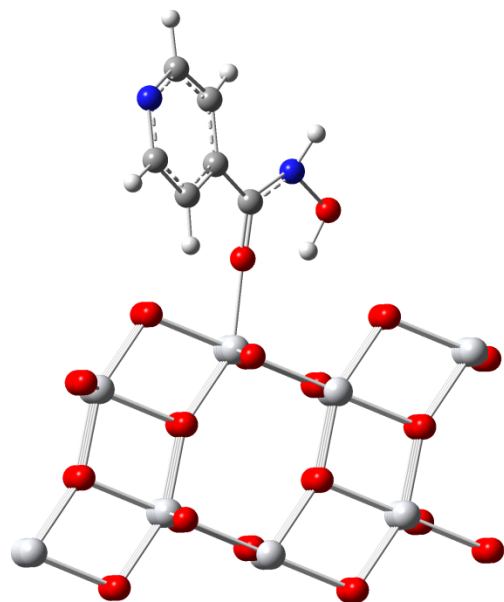
B6



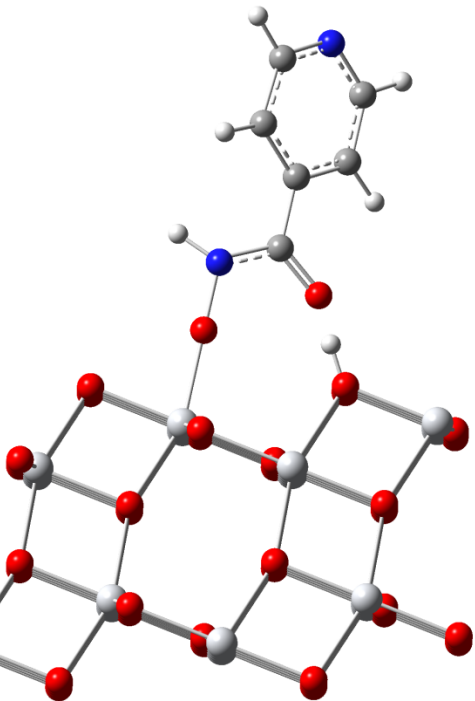
B7



B8



M1



M2

Figure S3 Evolution of anchoring bond lengths in configuration M3

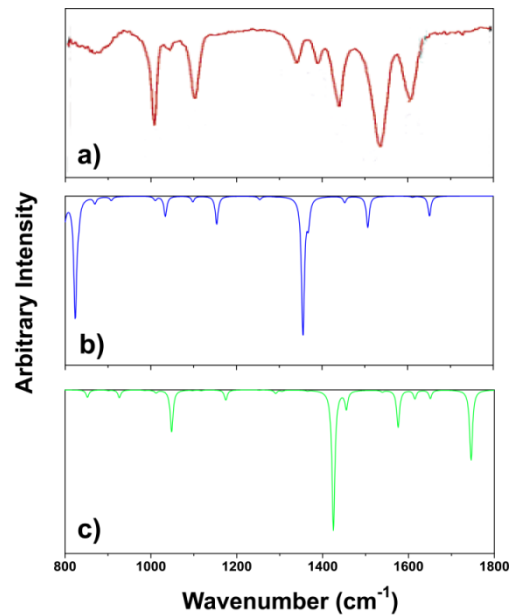


Figure S4. The experimental IR spectrum for acetohydroxamate (a) and calculated IR spectra for configuration B1 (b) and free anchor model (c)

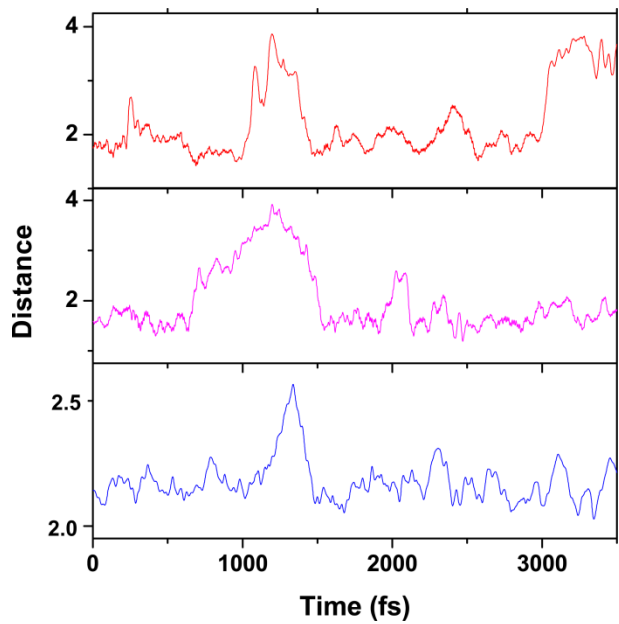


Fig. S5 Comparison of the EH and Kohn-Sham orbital gained from EH and DFT/B3LYP methods

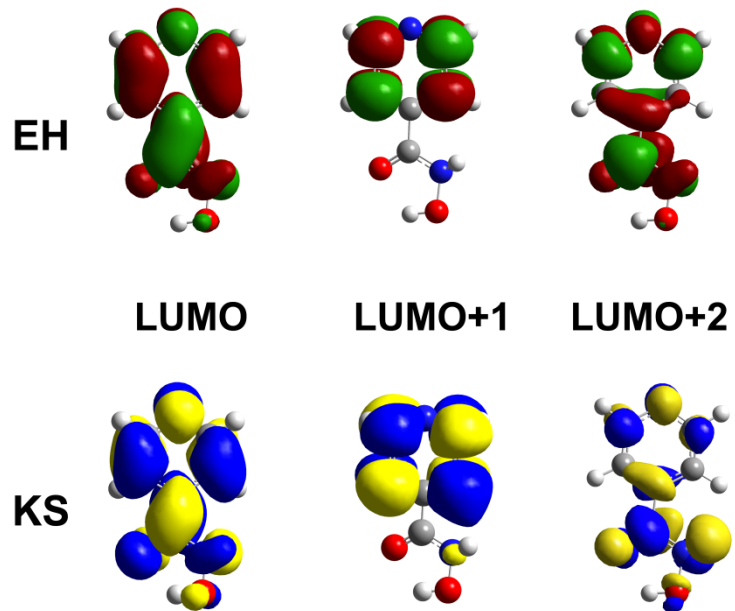


Fig. S6 Snapshots of the time-dependent charge distribution for B1

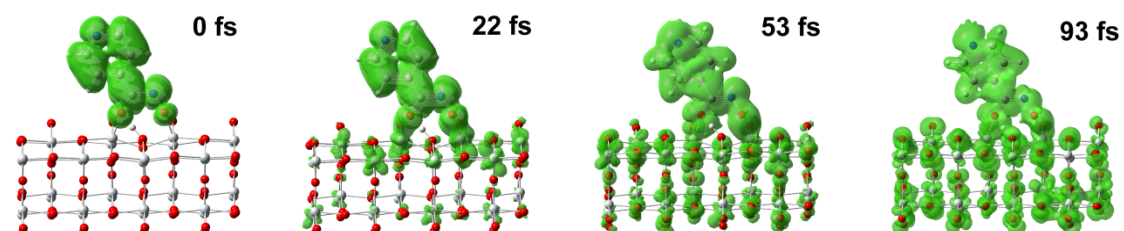


Figure S7 Illustrations of the LUMOs of the adsorbate and adsorbate/TiO₂ system

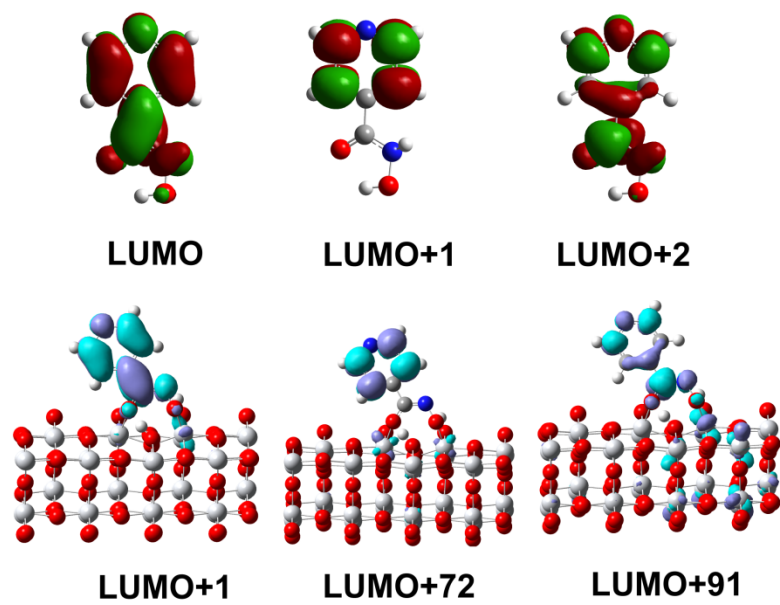


Table S1. The calculated and experimental wavenumber for the free and adsorbed models.

Adsorbed			Free		
Cal.	Exp.	Assign.	Cal.	Exp.	Assign.
823		$\delta(\text{O}_{2c}\text{-H})$	852	—	$\delta(\text{C-H})$
1034	1003	$\nu(\text{N-O})$	926	993	$\nu(\text{C-C}) + \delta(\text{N-H}) + \delta(\text{O-H})$
1153	1100	$\nu(\text{C-C}) + \delta(\text{C-H}) + \nu(\text{C=O}) + \nu(\text{N-O})$	1048	1092	$\nu(\text{N-O}) + \nu(\text{C-C}) + \delta(\text{N-H}) + \delta(\text{O-H})$
—	—	—	1174	—	$\nu(\text{C-C}) + \nu(\text{N-H})$
1355	1342	$\nu(\text{C=O}) + \nu(\text{C-C}) + \delta(\text{C-H})$	—	—	—
—	1391	—	—	1378	—
1452	1442	$\nu(\text{C=N}) + \delta(\text{C-H})$	1425	1450	$\delta(\text{N-H}) + \delta(\text{O-H}) + \nu(\text{C-C})$
1506	1539	$\nu(\text{C=N}) + \delta(\text{C-H})$	1576	1544	$\delta(\text{N-H}) + \delta(\text{O-H})$
1651	1611	$\delta(\text{C-H})$	1745	1638	$\nu(\text{C=O}) + \delta(\text{N-H}) + \delta(\text{O-H})$

Extended-Hückel (EH) method

The semiempirical Extended-Hückel (EH) method requires a small number of transferable parameters (1-9 parameters per atom), providing an excellent cost-benefit option for the accurate description of energy bands, chemical bonding, and quantum dynamic processes in very large extended systems. The EH tight-binding Hamiltonian has been extensively applied in studies of molecular and periodic systems, including several studies of sensitized TiO₂ surfaces.³⁻¹¹ The EH Hamiltonian is computed on the basis of the multi- ζ Slater-type orbitals (STO) for the radial part of the atomic orbital (AO) wave functions, with the 4s, 4p, and 3d atomic orbitals of Ti⁴⁺ ions, the 2s and 2p atomic orbitals of O²⁻ ions, the 2s and 2p atomic orbitals of C atoms, and the 1s atomic orbitals of H atoms. Having defined the atomic orbitals, the overlap and the Hamiltonian matrix elements can be computed, respectively, as $S_{ij} = \langle \phi_i | \phi_j \rangle$ and $H_{ij} = K' S_{ij} (H_{ii} + H_{jj}) / 2$. The diagonal elements H_{ii} correspond approximately to the valence-state ionization potential of the atomic species. In order to improve the accuracy of the EH method, a set of optimized Hückel parameters is used.

The Coulomb interaction between the photoexcited electron and hole pair

The Hamiltonian term H^{eh} accounts for the Coulomb interaction between the photoexcited electron and hole pair. According to the formalism, both wavepackets are written as a linear combination of Slater-type atomic orbitals, $|\Psi^{el}\rangle = \sum_i A_i^{el} |i\rangle$ and $|\Psi^{hl}\rangle = \sum_k A_k^{hl} |k\rangle$, with $\{|i\rangle\}$ and $\{|k\rangle\}$ spanning the atomic orbitals of the entire system. To account for the quantum dynamics of the wavepackets, A^{el} and A^{hl} are complex coefficients that depend on the time (not explicitly represented for clarity sake). The Coulomb energy of the electron–hole pair can be written as:

$$E_{el-hl} = \sum_{i,j} A_i^{*el} A_j^{el} \sum_{k,l} A_k^{*hl} A_l^{hl} \langle i,k | V_{coul} | j,l \rangle \quad (1)$$

Where $\langle i,k | V_{coul} | j,l \rangle$ are multicenter (2, 3, and 4) Coulomb integrals over Slater-type orbitals:

$$\langle i,k | V_{coul} | j,l \rangle = \int d\mathbf{r}_i^* \int d\mathbf{r}_j^* \chi_i^*(\mathbf{r}_i^*) \chi_k^*(\mathbf{r}_k^*) \frac{e^2}{|\mathbf{r}_i - \mathbf{r}_j|} \chi_l(\mathbf{r}_l) \chi_j(\mathbf{r}_j) \quad (2)$$

The Coulomb integrals, eq 2, are calculated by an efficient numerical algorithm adapted from the SMILES program for integrals with Slater-type orbitals. In our calculations, only the two-center Coulomb integrals are taken into account, because the threeand four-center integrals involving the electron–hole pair are much smaller and can be disregarded. The matrix elements for the electron wavepacket Hamiltonian, due to its interaction with the hole, are written as:

$$\begin{aligned} V_{ij}^{el} &= -A_i^{*el} A_j^{el} \sum_{k,l} A_k^{*hl} A_k^{hl} \langle i,k | V_{coul} | l,j \rangle \\ &= -A_i^{*el} A_j^{el} [\sum_k |A_k^{hl}|^2 \langle i,k | V_{coul} | l,j \rangle + 2 \sum_{k>l} \Re[A_k^{*hl} A_k^{hl}] \langle i,k | V_{coul} | l,j \rangle] \end{aligned} \quad (3)$$

and likewise for the hole wavepacket:

$$\begin{aligned}
V_{ij}^{hl} &= -A_j^{*hl} A_j^{hl} \sum_{k,l} A_k^{*el} A_k^{el} \langle i,k | V_{coul} | l,j \rangle \\
&= -A_i^{*hl} A_j^{hl} \left[\sum_k |A_k^{el}|^2 \langle i,k | V_{coul} | l,j \rangle + 2 \sum_{k>l} \Re e[A_k^{*hl} A_k^{el}] \langle i,k | V_{coul} | l,j \rangle \right]
\end{aligned} \tag{4}$$

If only the two-center Coulomb integrals are taken into account, A^{el} and A^{hl} are block diagonal matrices. During the excitonic dissociation and interfacial electron transfer, the electron wavepacket evolves under the influence of the Coulomb potential produced by the evolving hole and vice versa. The electron-hole coupling is described within the timedependent Hartree approximation. Exchange interaction effects are negligible because the wavepackets describe independent particles in this framework.

The procedure for quantum propagation of the photo-excited electron

The photo-excited electron is assumed to be initially localized in the adsorbate LUMO, and the time-evolved wave function $|\emptyset_i\rangle$ can be written as a liner combination of atomic orbitals:

$$|\emptyset(t)\rangle = \sum_{i,\alpha} B_{i,\alpha}(t) |i,\alpha\rangle \tag{5}$$

Where $|i,\alpha\rangle$ represents the atomic orbital α of atom i . The expansion coefficients $B_{i,\alpha}(t)$, introduced in eq 5, are computed according to:

$$B_{i,\alpha}(t) = \sum_q Q_{i,\alpha}^q C_q \exp\left(-\frac{i}{\hbar} E_q t\right) \tag{6}$$

after solving the generalized eigenvalue equation,

$$HQ^q = E_q S Q^q \tag{7}$$

Where H is the EH matrix and S is the overlap matrix in the atomic orbital basis. The coefficients C_q , introduced in eq 6, are defined by the expansion of the initial state in the orthonormal basis set of eigenvectors $|q\rangle$,

$$|\emptyset(0)\rangle = \sum_q C_q |q\rangle \tag{8}$$

The coefficients $Q_{i,\alpha}^q$, introduced in eq 6, are defined according to the expansion of the

eigenvectors $|q\rangle$ as a linear combination of atomic orbitals,

$$|q\rangle = \sum_{i,\alpha} Q_{i,\alpha}^q |i,\alpha\rangle \quad (9)$$

The projection of the time-evolved electronic wave function onto the atomic orbitals of the molecular adsorbate is, therefore, obtained according to the equation,

$$P(t) = \left| \sum_{i,\alpha}^{\text{MOL}} \sum_{i,\beta} B_{i,\alpha}^*(t) B_{j,\beta}(t) S_{\alpha,\beta}^{i,j} \right| \quad (10)$$

Here $S_{\alpha,\beta}^{i,j} = \langle i,\alpha | j,\beta \rangle$, where the indices α and β label specific orbitals in atoms i and j , respectively.

Note that the sum over j includes all of the atoms in the nanostructure, whereas the sum over i includes only atoms in the initially excited molecular adsorbate.

Frisch, M. J.; Trucks, G. W.; Schlegel, H. B.; Scuseria, G. E.; Robb, M. A.; Cheeseman, J. R.; Zakrzewski, V. G.; Montgomery, J. A., Jr.; Stratmann, R. E.; Burant, J. C.; Dapprich, S.; Millam, J. M.; Daniels, A. D.; Kudin, K. N.; Strain, M. C.; Farkas, O.; Tomasi, J.; Barone, V.; Cossi, M.; Cammi, R.; Mennucci, B.; Pomelli, C.; Adamo, C.; Clifford, S.; Ochterski, J.; Petersson, G. A.; Ayala, P. Y.; Cui, Q.; Morokuma, K.; Malick, D. K.; Rabuck, A. D.; Raghavachari, K.; Foresman, J. B.; Cioslowski, J.; Ortiz, J. V.; Stefanov, B. B.; Liu, G.; Liashenko, A.; Piskorz, P.; Komaromi, I.; Gomperts, R.; Martin, R. L.; Fox, D. J.; Keith, T.; Al-Laham, M. A.; Peng, C. Y.; Nanayakkara, A.; Gonzalez, C.; Challacombe, M.; Gill, P. M. W.; Johnson, B. G.; Chen, W.; Wong, M. W.; Andres, J. L.; Head-Gordon, M.; Replogle, E. S.; Pople, J. A. *Gaussian 09*, Revision D.01; Gaussian Inc.: Wallingford CT, 2009.

References

1. Nilsing, M.; Persson, P.; Ojamae, L. Anchor group influence on molecule-metal oxide interfaces: Periodic hybrid DFT study of pyridine bound to TiO₂ via carboxylic and phosphonic acid. *Chem Phys Lett* **2005**, *415* (4-6), 375-380.
2. Nilsing, M.; Lunell, S.; Persson, P.; Ojamae, L. Phosphonic acid adsorption at the TiO₂ anatase (101) surface investigated by periodic hybrid HF-DFT computations. *Surf Sci* **2005**, *582* (1-3), 49-60.
3. Bowman, D. N.; Blew, J. H.; Tsuchiya, T.; Jakubikova, E. Elucidating band-selective sensitization in iron(II) polypyridine-TiO₂ assemblies. *Inorg Chem* **2013**, *52* (15), 8621-8.
4. Bairu, S. G.; Mghanga, E.; Hasan, J.; Kola, S.; Rao, V. J.; Bhanuprakash, K.; Giribabu, L.;

- Wiederrecht, G. P.; da Silva, R.; Rego, L. G. C.; Ramakrishna, G. Ultrafast Interfacial Charge-Transfer Dynamics in a Donor-pi-Acceptor Chromophore Sensitized TiO₂ Nanocomposite. *J Phys Chem C* **2013**, *117* (9), 4824-4835.
5. Hoff, D. A.; da Silva, R.; Rego, L. G. C. Coupled Electron-Hole Quantum Dynamics on D-pi-A Dye-Sensitized TiO₂ Semiconductors. *J Phys Chem C* **2012**, *116* (40), 21169-21178.
 6. Hoff, D. A.; Silva, R.; Rego, L. G. C. Subpicosecond Dynamics of Metal-to-Ligand Charge-Transfer Excited States in Solvated [Ru(bpy)₃]²⁺Complexes. *The Journal of Physical Chemistry C* **2011**, *115* (31), 15617-15626.
 7. Rego, L. G. C.; da Silva, R.; Freire, J. A.; Snoeberger, R. C.; Batista, V. S. Visible Light Sensitization of TiO₂ Surfaces with Alq₃ Complexes. *J Phys Chem C* **2010**, *114* (2), 1317-1325.
 8. da Silva, R.; Rego, L. G. C.; Freire, J. A.; Rodriguez, J.; Laria, D.; Batista, V. S. Study of Redox Species and Oxygen Vacancy Defects at TiO₂-Electrolyte Interfaces. *J Phys Chem C* **2010**, *114* (45), 19433-19442.
 9. Rego, L. G. C.; Santos, L. F.; Batista, V. S. Coherent Control of Quantum Dynamics with Sequences of Unitary Phase-Kick Pulses. *Annu Rev Phys Chem* **2009**, *60*, 293-320.
 10. Abuabara, S. G.; Rego, L. G. C.; Batista, V. S. Influence of thermal fluctuations on interfacial electron transfer in functionalized TiO₂ semiconductors. *J Am Chem Soc* **2005**, *127* (51), 18234-18242.
 11. Rego, L. G. C.; Batista, V. S. Quantum dynamics simulations of interfacial electron transfer in sensitized TiO₂ semiconductors. *J Am Chem Soc* **2003**, *125* (26), 7989-7997.